Appl. Phys. B 71, 673–680 (2000) / Digital Object Identifier (DOI) 10.1007/s003400000408

Applied Physics B
Lasers
and Optics

Mid-infrared laser-induced grating experiments of C_2H_4 and NH_3 from 0.1–2 MPa and 300–800 K

M. Gutfleisch[1], **D.I. Shin**[1], **T. Dreier**[1], **P.M. Danehy**[2]

[1] Physikalisch Chemisches Institut, Universität Heidelberg, Im Neuenheimer Feld 253, 69120 Heidelberg, Germany
[2] The Australian National University, Department of Physics, Science Faculty, Canberra, ACT 0200, Australia

Received: 17 March 2000/Revised version: 23 March 2000/Published online: 13 September 2000 –

Abstract. Laser-induced thermal gratings (LITG) were generated in mixtures of ethylene and ammonia in nitrogen using mid-infrared laser radiation from a grating-tuned, low-pressure, pulsed (5 ms pulse width) CO_2 laser, and read out with a continuous wave Nd:YLF laser. The LITG signal intensity was measured as a function of pressure (0.1–2 MPa) and temperature (300–800 K, at 0.1 and 1 MPa) by tuning the laser to the accidental coincidences of the 10P(14) and 10R(6) emission lines with molecular absorption transitions of C_2H_4 and NH_3, respectively. Comparisons are made with theoretical predictions for the grating efficiency from a simple thermalization model. A theoretical comparison of the temporal LITG signal response for three excitation pulse shapes – a delta function, a realistic pulse, and a square wave is presented. Furthermore, it is shown that for NH_3, most of the decrease of the LITG signal intensity with increasing temperature is due to the corresponding decrease in fractional molecular absorption of the pump beam radiation. The diagnostic capabilities of the mid-infrared LITG experiment is demonstrated for spatially resolved ethylene measurements with long laser pulses in a premixed stoichiometric CH_4–air flame at atmospheric pressure.

PACS: 42.62.Fi; 43.35.Ae; 51.20.+d

In laser-induced thermal grating (LITG) experiments a probe laser beam which is fully transmitted by the sample (non-absorbing at wavelength λ_{pr}) is partially reflected off a sinusoidally modulated thermal grating structure in the gaseous medium formed initially by the intensity interference pattern of two crossed pulsed laser beams at wavelength λ_p. In the case of excitation of infrared-active vibrations in a molecule the cause of this refractive index change is heat release to the surrounding medium via fast equilibration of vibrational energy between neighboring vibrational modes in the excited species and slower vibration-translational (VT) relaxation which can launch acoustic sound waves and a slowly decaying density modulation in the interaction region of the beams [1, 2].

In the past many applications of laser-induced gratings in the gas phase involved electronic states with fast collision-induced radiationless quenching of the excitation energy to generate the thermal grating structure in, for example, NO_2 [3–5], NO [3, 6] and OH [7, 8]. It was shown that the LITG technique is a sensitive spectroscopic probe for gas-phase species. In addition, the method allows the measurement of transport properties of the bulk medium and temperature via the adiabatic velocity of sound using laser pulses of short duration (tens of ns).

The present work explores the applicability of laser-induced thermal grating spectroscopy in the mid-infrared spectral region for the spatially resolved detection of hydrocarbons (C_2H_4) and amines (NH_3) in gaseous samples under controlled conditions as well as flame environments. This is a continuation of our previous study for ethylene performed at room temperature [9]. Both species are of importance in air-fed combustion processes both as fuels and pollutants. A CO_2 laser with a pulse duration of several ms is used as the excitation source. This time is long in comparison with energy relaxation times within the molecules as well as diffusional motion in the gaseous sample. The temperature and pressure dependence of the LITG signal intensity is investigated and compared with a simple theoretical model to describe the underlying excitation and relaxation processes as a function of these parameters. With this model the time development of the LITG signal intensity can qualitatively be reproduced for the present experimental conditions. The results obtained demonstrate that LITG is a sensitive combustion diagnostic tool for spatially resolved monitoring of species with intrinsically low fluorescence quantum yield, which therefore are less favorably probed by laser-induced fluorescence (LIF).

1 Theoretical description

The main difference between the experiments described below and previous laser-induced grating measurements is the long pulse width (5 ms) of the employed CO_2 laser. It is used

This work is dedicated to Prof. J. Wolfrum on the occasion of his 60th birthday.

to excite rovibrational Q-branch transitions in the ν_7 bending mode of C_2H_4 [10] or the ν_2 tunneling mode of NH_3 [11], respectively. Table 1 shows that for the total pressures used here (0.1–2 MPa) intramolecular vibration–vibration energy exchange as well as collisional vibration–translation (V–T) relaxation transfer are both fast processes compared with the laser pulse duration τ_L, and the thermal diffusion time, τ_{th} [1, 12, 13]. The deposition of translational energy as heat in the medium gives rise to a thermal grating, which is detected by deflection of a continuous wave probe beam at wavelength λ_{pr} directed into the interaction region at the Bragg angle ϕ_B, with $\sin\phi_B = \lambda_{pr}/2\Lambda$. The intensity grating is characterized by a wavevector $\boldsymbol{q}$, with $|\boldsymbol{q}| = 2\pi/\Lambda$ perpendicular to the grating planes with wavelength $\Lambda = \lambda_p/(2\sin(\theta/2))$, where θ is the crossing angle between the two pump beams.

The model described below for calculating the LITG signal intensity, as adopted from Eichler et al. [1] and Danehy et al. [6], only holds in the limit of high Reynolds numbers (with the grating spacing as the relevant length scale and the sound speed, v, as the velocity) so that acoustic energy is not deposited in the probe volume. For our conditions, $\mathrm{Re} = \varrho v/\mu = 4430$ at 1 atmosphere and 300 K. We assume that the timescale for thermal diffusion is short compared with the pump laser pulse duration ($\tau_L \gg \tau_{th} = 1/(q^2 D)$), where $D = \kappa/\varrho c_p$ is the thermal diffusivity, κ is the thermal conductivity, ϱ is the gas density and c_p is the specific heat at constant pressure. Furthermore, the decay times for collision-induced deactivation of excitation energy in the molecular ensemble (V–V, V–T, R–T relaxation) is small compared with the laser pulse duration ($\tau_{VT} \ll \tau_L$). This condition ensures that the rate of energy addition follows the laser pulse shape. A final assumption is that the laser pulse duration is long compared to the characteristic acoustic time $\tau_a = \Lambda/v$. If $\tau_L \ll \tau_a$, then a pair of counterpropagating traveling acoustic waves are generated impulsively by the laser. These waves beat with each other, causing density modulations that contribute to and modulate the LITG signal which allows measurement of the gas sound speed. If $\tau_L \gg \tau_a$ as is the case in the present experiment, then the beating, counterpropagating acoustic waves are not generated which simplifies the theoretical analysis significantly. The relevant timescales of the problem are summarized in Table 1. This table shows that all of the above assumptions are satisfied in the current experiment.

Population – and thermal – gratings both change the complex refractive index $n = n' + i\alpha$ of the medium by $\Delta n'$ and $\Delta\alpha$, which both determine the scattering efficiency η for the probe laser beam [1]

$$\eta \frac{I_{sig}}{I_{probe}} = \left(\frac{\pi L \Delta n'}{\lambda_{pr}}\right)^2 + \left(\frac{L\Delta\alpha}{4n}\right)^2 , \quad (1)$$

where L is the "length" of the interaction volume. In the present experiment, the grating is read out using a nonresonant probe laser. Thus, contributions from population gratings can be neglected. Consequently, the second term in (1) is ignored. For small density perturbations ($\Delta\varrho \ll \varrho_0$) and assumption of ideal gas behavior, the refractive index change $\Delta n'$ can be written as [6]

$$\Delta n' = \left(\frac{\partial n}{\partial \varrho}\right)_T \Delta\varrho , \quad (2)$$

if the temperature variation of n at constant density is neglected. With the long pump pulses in our experiment there is no impulsive heating of the surrounding gas and the pressure increase from heat addition is continuously being radiated away. Therefore, an isobaric heat addition is an appropriate assumption, and one may write

$$\Delta\varrho = -\varrho_0 \frac{\Delta T}{T_0} . \quad (3)$$

The temporal development of the temperature perturbation can be deduced from solving

$$\frac{\mathrm{d}\Delta T(t)}{\mathrm{d}t} + \frac{\Delta T(t)}{t_{th}} = \frac{2\alpha}{\varrho c_p}\Delta I(t) , \quad (4)$$

where thermalization of absorbed energy is assumed fast, α is the absorption coefficient and $\Delta I(t)$ is the temporal development of the grating intensity modulation which is directly related to the intensity of the grating-forming laser. For an arbitrary-shaped laser pulse, (4) can be solved numerically. This numerical approach is adopted in the analysis of the temporal evolution of the LITG signal in this paper. Figure 1 shows calculated temporal LITG signal traces for three different excitation laser pulse shapes, a δ-function, our measured experimental pulse profile, and a square (top-hat) input, all exhibiting the same total energy. In this comparison, the δ-function laser generates 3.3 times more signal (integrated over time) than the square wave. The measured pulse generates 1.3 times more signal than the square wave input. But, these exact ratios depend on the choice of the thermal diffusion time constant.

Figure 2 shows the development of the LITG signal trace with increasing sample pressure (equivalent to increasing τ_{th}) calculated from (1)–(4), using the measured excitation laser pulse, and assuming a continuous-wave probing beam. All the curves are normalized to their peak amplitude. The progressively slower decay of the signal amplitude with increasing pressure is clearly visible.

A simple scaling law for the LITG signal can be derived for the case of a square pulse of duration τ_{Ls}, where $\tau_{Ls} \gg \tau_{th}$. In this case, the solution of (4) can be performed analytically [1]:

$$\Delta T = \Delta T_{st}(1 - \mathrm{e}^{-t/\tau_{th}}) \quad t \le \tau_L ,$$
$$\Delta T = \Delta T(\tau_L)\,\mathrm{e}^{(-t-\tau_L)/\tau_{th}} \quad t > \tau_L , \quad (5)$$

Table 1. Estimated values for the time constants [μs] for thermal diffusion (τ_{th}), acoustic transit (τ_a) and mass diffusion (τ_d) involved in the generation and destruction of thermal gratings at three different pressures. For τ_{VT}, the time constant for vibration-translational relaxation, the first entry is for C_2H_4/Ar [13] and the second entry is for NH_3/N_2 [20] collision pairs, respectively. Thermophysical parameters for pure nitrogen were used in calculating the pressure dependence of the respective time constants: $\varrho = 1.142\,\mathrm{kg/m^3}$, $c_p = 1.041\,\mathrm{kJ/(kg\,K)}$, $\kappa = 0.026\,\mathrm{W/(m\,K)}$, $v_s = 353.2\,\mathrm{m/s}$, $\eta = 1.79\times10^{-6}\,\mathrm{kg/(m\,s)}$, $\gamma = 1.4$, $D_{12} = 0.17\times10^{-4}\,\mathrm{m^2/s}$

Pressure /MPa	τ_{th}	τ_a	τ_d	τ_{VT}
0.15	66	0.56	86	1.8/0.073
1.00	437	0.56	572	0.26/0.011
2.20	961	0.56	1259	0.12/0.005

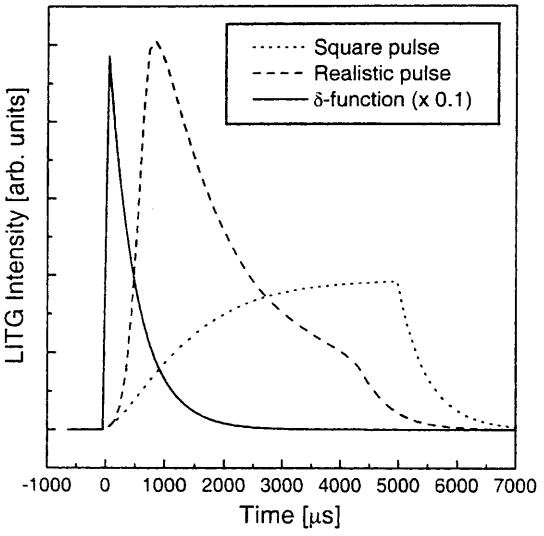

Fig. 1. Temporally resolved LITG signal amplitude by solving (4) for three different assumed excitation laser pulse shapes: A δ-function (*solid line*; intensity divided by 10), the measured pulse shape for the present experiment (*dashed line*), and a square pulse (*dotted line*). All input pulses have the same total energy. Assumed total pressure is ≈ 0.1 MPa ($\tau_{th} = 1000\,\mu$s)

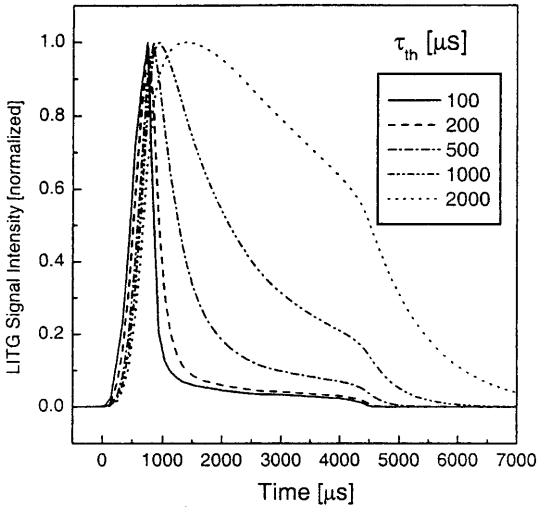

Fig. 2. Theoretically calculated temporal LITG signal profiles by solving (4) numerically with the measured excitation pulse used in the experiment (see Fig. 6) for increasing pressure, i.e., increasing thermal diffusion time constant τ_{th}

with

$$\Delta T_{st} = \frac{2\alpha\Delta I}{\kappa q^2}\,, \tag{6}$$

which is the amplitude of the temperature modulation in the steady-state limit. For the case of the square pulse shape, the numerical solution of (4), shown in Fig. 1, compares very well with the analytical solution given by (5).

To obtain a closed-form solution for use as a scaling law, further assumptions are required. First, we assume that both grating-forming lasers are of equal intensity. Second, we again invoke $\tau_{Ls} \gg \tau_{th}$ to ignore the short rising and falling edges of the LITG signal. Under these conditions, (1)–(6) can be combined to produce an expression for the LITG signal intensity:

$$I_{sig}(t) = \left[\left(\frac{\partial n}{\partial \varrho}\right)_T\right]^2 \left(\frac{p\varepsilon(p)\sigma(p)\Delta N_0 I(t) L \Lambda^2}{2\lambda_{pr}\kappa R T^2 \pi}\right)^2 I_{pr}\,. \tag{7}$$

The absorption coefficient α has been replaced by the corresponding absorption cross section via $\alpha = \sigma\Delta N_0$ for a two-level model. Here, ΔN_0 is the difference between ground and excited states in the number density of the absorbing molecules. Also, a pressure-dependent energy deposition efficiency term $\varepsilon(p)$ which is always less than or equal to unity has been added, following Danehy et al. [6]. Inspection of (7) reveals a $p^2\sigma^2/T^4$ dependence of the registered LITG signal intensity from the parameters pressure, absorption cross section and temperature, respectively. In the present static-cell experiments, the number density of absorbers is held constant, but the fraction of the molecules in the state probed (Boltzmann fraction) varies with temperature as well. Equation (7) only holds for the excitation laser tuned to line center of an isolated absorption transition, both of which are poor approximations in the present experiments.

The pressure and temperature dependences shown by (7) differ from the derivation in Danehy et al. [6], who assumed excitation by a short laser pulse with $\tau_L\delta \ll \tau_d$, where $\tau_L\delta$ is the duration of the delta function laser pulse. Following Eichler et al. [1] one can directly compare derivations based on these differing assumptions to show that $I_{sig\text{-}square}/I_{sig\text{-}delta} = (\tau_{th}/\tau_L\delta)^2$. This has some important implications. Since τ_{th} is proportional to gas density, the ratio of peak signals scales as p^2/T^2. Thus, the square pulse laser might be more advantageous in higher pressure situations. For the same experimental conditions (same τ_{th}) the square pulse is predicted to have much larger peak intensity compared to the delta-function pulse, assuming equal laser intensity used in both experiments. The assumption of equal laser intensity used here is more realistic than the assumption of equal laser energy used in Fig. 1, because in experiments, the maximum intensity is limited by transition saturation.

One can compute time-integrated signal intensities, S_{sig}, from:

$$S_{sig} = \int_0^\infty I_{sig}(t)\,\mathrm{d}t\,. \tag{8}$$

Comparing the square pulse and the delta pulse, we find $S_{sig\text{-}square}/S_{sig\text{-}delta} = 2\tau_{th}\tau_{Ls}/\tau_L\delta^2$. Again, the ratio of time-integrated signals increases with pressure and decreases with temperature, but not as dramatically as in the case of peak intensities. By integrating the signals over the duration of the pulse, the signal ratio is dramatically increased. This analysis suggests that there are several advantages to using a long-pulsed laser, such as was the case in the present experiment.

2 Experimental setup

The experimental setup is essentially identical to the one described previously [9] and is depicted in Fig. 3. Briefly, the two grating forming beams were provided by splitting the output beam of a low pressure (1.6 kPa) pulsed CO_2

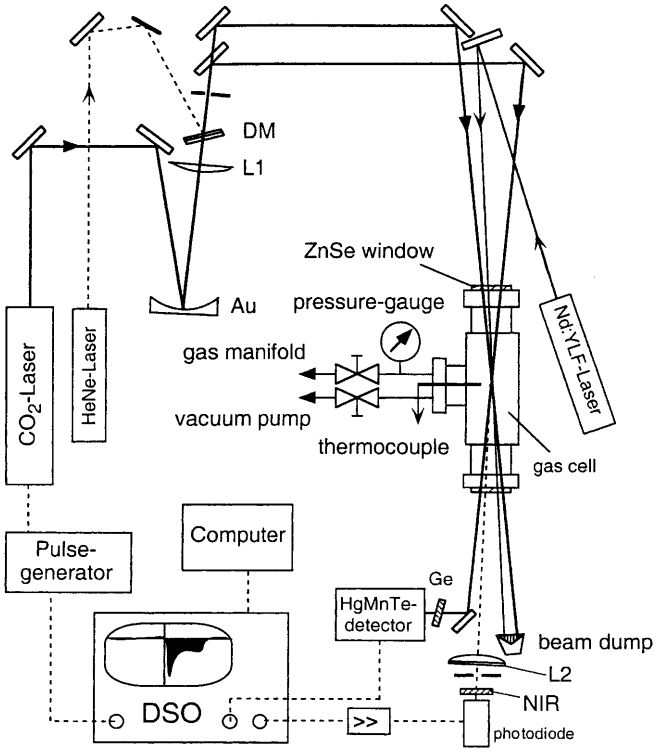

Fig. 3. Experimental arrangement for laser-induced grating measurements in gaseous samples and flames using a pulsed CO_2 laser for excitation and a cw Nd:YLF laser for probing the thermal grating. The He-Ne laser is for prealignment of the infrared beams. L1: ZnSe lens, DM: dielectric coated ZnSe beam combiner, Au: gold-coated mirror, Ge: germanium flat, L2: quartz lens, NIR: near-infrared longwave pass filter

laser (Edinburgh Instruments, PL6), which operated on discrete transitions in the 10-μm band through a grating in Littrow mount. The temporal pulse shape is structured, with a short (duration < 1 ms) peak at the beginning of the pulse and a slowly decaying tail (duration: ≈ 4 ms) with an amplitude of roughly 25% of the first peak. Typical output energies at a 10-Hz repetition rate were 220 mJ per pulse, with a nearly Gaussian beam profile of diameter 7.3 mm FWHM at a distance of 2 m behind a demagnifying telescope. The two beams were split with an intensity ratio of 3:2 and crossed with an angle of $(3.1 \pm 0.5)°$. The temporal pulse shape of the pump laser was monitored with a liquid-nitrogen-cooled HgMnTe detector (EG&G Judson) with a time constant of 0.5 μs and a digital storage oscilloscope (DSO, Gould, 200 MHz bandwidth). The probe beam was delivered from a diode pumped Nd:YLF laser at $\lambda_{pr} = 1053$ nm (Spectra Physics, Mod. T20-FD) with a variable continuous wave output power between 0.1–4 W. The probe beam was coupled into the sample volume under the phase matching angle of 0.16°. The diffracted signal beam, after being focused through a small-diameter (0.5 mm) aperture, was detected by a Si photodiode through a long-pass filter (Schott, RG 830). Reported signal intensities are peak (not time-integrated) intensities measured from the DSO. The temporal LITG signal traces were captured, averaged and stored in the DSO. The time response of the LITG detector to a 10-ns Nd:YAG laser pulse exhibited a time constant of 127 μs, which, as described below, was not fast enough to temporally resolve finer details of the LITG signal. Optical prealignment was performed with a He-Ne laser coupled into the IR beam path via a coated ZnSe dichroic beam combiner (DM in Fig. 3).

Temperature-dependent LITG signal intensities were acquired in a vacuum and pressure-tight heated stainless steel sample cell equipped with ZnSe windows for optical access. Cooling of the window flanges was accomplished by flowing water through tightly fitting copper tubing. A pressure manometer, a gas manifold/vacuum pump and a thermocouple for temperature regulation were connected to the cell body through separate fittings.

Measurements were also performed in premixed methane/air flames stabilized on a Bunsen burner [14]. The burner consisted of a 10-mm-diameter water-cooled central tube (1 m long) which provided the fuel-air mixture, and a concentric annular tube (opening diameter 32 mm) for optional nitrogen coflow. Typical gas flow rates were 0.47 and 5.04 slm (standard liter per minute) CH_4 and air, respectively, resulting in a flow speed of 117 cm/s at the exit of the tube. The coflowing air flow was about 100 slm. The whole burner assembly could be vertically translated with sub-millimeter resolution relative to the laser beam axis by a mechanical drive.

3 Results

3.1 Temperature dependence of LITG signal intensities

To study the behavior of the LITG signal intensities as a function of temperature for 0.1 and 1 MPa total pressure, mixtures were prepared of the absorbing species with nitrogen (1% C_2H_4 or NH_3 by partial pressure) in the static cell. For efficient excitation of ethylene and ammonia the CO_2 laser was tuned to the 10P(14) (949.67 cm^{-1}) and 10R(6) (966.18 cm^{-1}) line of CO_2, respectively [15, 16].

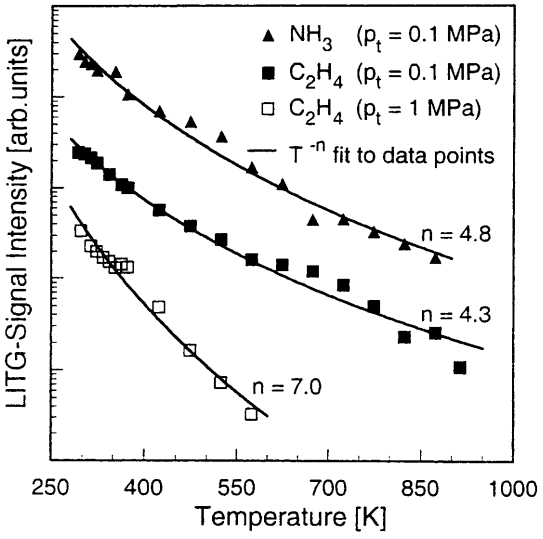

Fig. 4. Variation with temperature of the LITG signal intensity in the static nitrogen gas mixtures. The partial pressure of C_2H_4 (*filled square*) and NH_3 (*filled triangle*) is 0.1 kPa and 0.5 kPa, respectively, at a total pressure of 0.1 MPa. The temperature dependence for C_2H_4 was also determined at 1 MPa total pressure (*open squares*). Also shown are T^{-n} (*n* indicated for each plot) temperature dependencies (*solid lines*) which best fitted the experimental data

Figure 4 summarizes the temperature dependence of the LITG signal intensities obtained for both species in the cell experiments at total pressures of 0.1 MPa (filled symbols) and 1 MPa (open symbols), respectively. Since absolute signal intensities have to be determined for each temperature series (which took several hours because of equilibration of the mixtures) any variation in laser performance (pulse energy, beam profile and beam overlap) during this measurement period will influence the result, which explains most of the scatter in the data points. Nevertheless, reasonable T^{-n} temperature fits (shown as solid lines in Fig. 4) were obtained to describe the temperature variation of the signal intensity for each species. It can be seen that for the experiments at 0.1 MPa the best fit exponents n are close to the value of 4 as predicted from the simple theory presented above for the thermal grating signal intensity of a two-level atom at $I \ll I_{\mathrm{sat}}$, for example (7). This close agreement, however, is fortuitous, since effects such as energy level population as well as spectral line overlap and excitation of the transitions in the vicinity of the CO_2 laser excitation line are not considered in the theory (see, however, the discussion section). Certainly, the C_2H_4 data at 1 MPa deviate strongly from the T^{-4} power law.

3.2 Pressure dependence of LITG signal intensities

The effect of pressure on the LITG signal intensity was investigated in the range 0.03–2 MPa for temperatures of 320 and 410 K, respectively. For each temperature the cell first was filled with 1.1 kPa of ethylene, and then nitrogen was added until the final pressure was reached. The results of both experimental runs are presented in Fig. 5 in a double logarithmic plot. Similar to our previous investigations in C_2H_4/N_2 mixtures at room temperature [9] the signal increases with pressure at the higher temperatures investigated in this work. Best fit straight lines to the data yield a p^n pressure dependence of the LITG signal intensity with exponents n equal to 0.95 and 1.5, respectively, for 320 and 410 K.

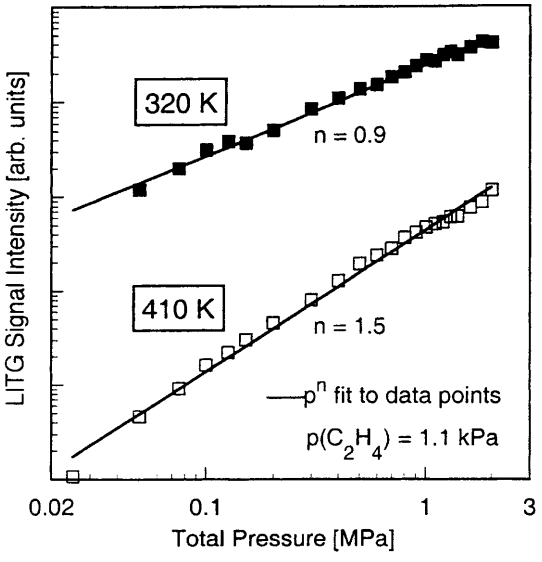

Fig. 5. Pressure dependence of the LITG signal intensity from samples containing 1.1 kPa C_2H_4 at a gas temperature of 320 (*filled squares*) and 410 K (*open squares*), respectively

3.3 Temporal evolution of signal intensity

To illustrate the change in the time behavior of the LITG signal with increasing pressure we plotted in Fig. 6, together with the excitation laser pulse shape (dashed line), the temporal shape of the measured photodiode current at three different pressures. Even though with the present experimental setup we were unable to resolve the detailed temporal characteristics of the scattered signal beam it can clearly be seen that the signal no longer follows the temporal profile of the pump laser pulse. Instead, the signal decay gets slower, and the ratio of the first peak to the trailing shoulder decreases with increasing pressure. These observations reflect the slowing down of the thermal diffusional processes which dissipate the thermal energy by washing out the grating structure.

3.4 Flame measurements

To demonstrate the feasibility of mid-infrared thermal grating spectroscopy for flame diagnostics we used the present experimental setup for spatially resolved detection of ethylene seeded into a premixed flame stabilized on a Bunsen burner. Figure 7 shows the LITG signal intensity from C_2H_4 (1.2% of total flow) obtained in a slightly lean ($\phi = 0.93$) CH_4–air flame as a function of height above the tube exit. Reasonable LITG signals were only obtained within the inner flame cone up to a height of 13 mm. Judging from the known temperature profile of this flame along the central tube axis [14] the flame front is located approximately at 16 mm from the burner exit. Up to this height almost all fuel in the fresh gas should be consumed, at least to a residual concentration level below the present LITG detection limit (see below) at flame temperatures of 2100 K [17]. The observed decrease of the signal intensity is partly due to the temperature dependence of the fractional population in the absorbing level, dilution effects in the flame gases, and possible destruction of the detected species through pyrolysis and oxidation at higher temperatures closer to the flame tip. In addition, the

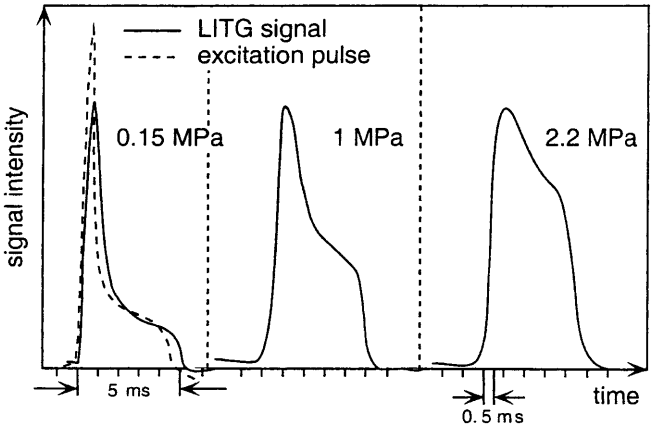

Fig. 6. Temporally resolved LITG signal intensity profiles (*solid lines*; normalized to the same peak value) recorded with the present detector/oscilloscope combination. The cell contained a 1.1% ammonia/nitrogen mixture at 300 K at total pressures of 0.1, 1 and 2.2 MPa, respectively. The temporal profile of the CO_2 laser pulse registered by the cooled HgMnTe detector is plotted as a *dashed line*

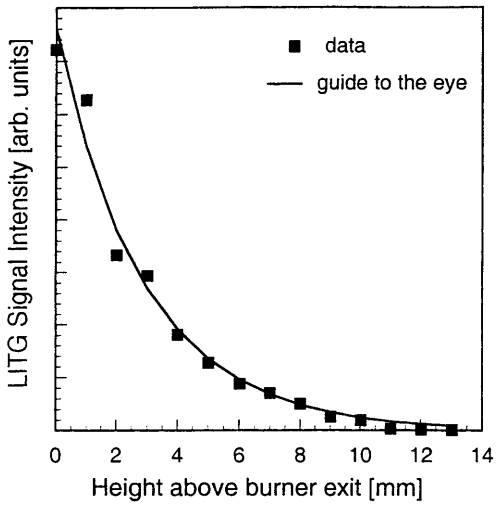

Fig. 7. LITG signal intensity of C_2H_4 in a premixed methane/air flame as a function of height above the exit of the inner tube of the Bunsen burner. The flame was operated slightly lean ($\phi = 0.93$) with 1.2% C_2H_4 seeded into the premixed gas flow. The tip of the visible inner flame cone was at 16 mm above the tube opening

present crossing angle of the pump beams causes the spatial sampling length to be large in comparison to the flame dimensions close to the tip, which means that the effective volume containing the probed species is decreasing. In the crossed-beam setup of Fig. 3 the spatial resolution transverse to the focused beams was estimated to $\pm 500\,\mu$m. However, due to the small crossing angle the spatial resolution is less in the direction parallel to the beams. We have determined the spatial response function of the present setup by translating a thin sheet of a C_2H_4 (1% in nitrogen) flow emanating from a 1-mm-wide slit nozzle through the interaction region along the beam propagation direction (see Fig. 8). If one defines the $1/e$ intensity points of the detected LITG signal as a criterion for the size of the sampling length, this would amount to ± 2.5 mm.

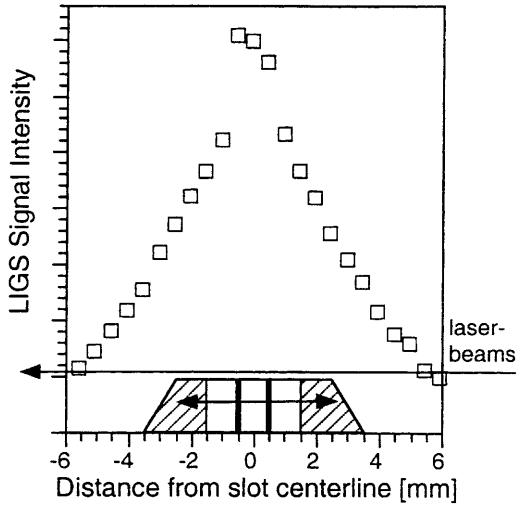

Fig. 8. Determination of the spatial resolution of the LITG probe volume by recording the LITG signal intensity (*open squares*) while a thin sheet flow of C_2H_4 in nitrogen from a 1-mm-wide slit nozzle was translated through the laser beam interaction region

3.5 Detection sensitivity

With a gradual dilution of initially 650 ppm of the absorbing species in nitrogen we estimated a detection sensititvity ($S/N \approx 2$) of 20 ppm for C_2H_4 at 300 K and 1 bar total pressure. This lower limit increased to 80 ppm and 38 ppm at a cell temperature of 770 K and at a total pressure of 1 and 10 bar, respectively. In the flame the detection limits for C_2H_4 and NH_3 of 415 and 126 ppm, respectively, were determined from systematically decreasing the corresponding flow of these seed gases through calibrated flow controllers and observing the signal-to-background ratio.

4 Discussion

It is obvious that during and after the long excitation pulse employed in the present experiments a two-level relaxation model approach is not adequate to describe the complex excitation/relaxation pathways for ethylene and ammonia at higher pressures and as a function of temperature. The broadening coefficients for homogeneous line broadening are estimated to be $\gamma_{C_2H_4} = 0.16\,\mathrm{cm^{-1}atm^{-1}}$ [18] and $\gamma_{NH_3} = 0.094\,\mathrm{cm^{-1}atm^{-1}}$ [11, 16], respectively, with a corresponding spectral overlap of neighboring transitions. For a detailed modeling the spread in population distribution throughout the ground state level manifold with increasing temperature (due to the strong temperature dependence of the partition function) has to be considered as well.

According to (7) one parameter that determines the LITG signal intensity is the squared absorption coefficient α of the sampled transition at the frequency of the pump beam radiation, which in general is a function of temperature and pressure. To calculate the temperature dependence of α for ammonia at 0.1 MPa in the spectral overlap region with the 10R(6) CO_2 laser line centered at $966.18\,\mathrm{cm^{-1}}$ we used the HITRAN software package [11]. For our low-pressure CO_2 laser we assumed a Lorentzian line profile with a FWHM of $5 \times 10^{-3}\,\mathrm{cm^{-1}}$ [16]. In the simulation of $\alpha(v, T)$ a constant homogeneous line broadening coefficient of $\gamma_{NH_3} = 9.3 \times 10^{-4}\,\mathrm{cm^{-1}\,kPa^{-1}}$ [16] with a $T^{-0.75}$ temperature dependence was assumed for all considered transitions in the neighborhood of the exciting CO_2 laser line. The total absorption is then obtained by integration of α for each temperature over the spectral distribution $I_L(v)$ of the incoming laser light [16]:

$$\alpha' = \int_{v-\Delta}^{v_0+\Delta} I_L(v)\alpha(v)\,\mathrm{d}v\,. \tag{9}$$

The Doppler width was estimated to be 2.2×10^{-3} and $3.7 \times 10^{-3}\,\mathrm{cm^{-1}}$ at 300 and 800 K, respectively. If the contributions from all NH_3 transitions in the 965–967 $\mathrm{cm^{-1}}$ range which contribute to absorption within the CO_2 laser emission profile are considered for the calculation the temperature-dependent absorption of the pump beam radiation in the sample can then be well represented by a $T^{-1.6}$ power law in the 300–900 K range. If one considers the proportionality of the LITG signal intensity with $(\alpha')^2$ this reduced fractional absorption of the pump beams in the interaction region is reflected by $T^{-3.2}$ a temperature dependence, which is depicted in a linear plot in Fig. 9 together with the experimental data

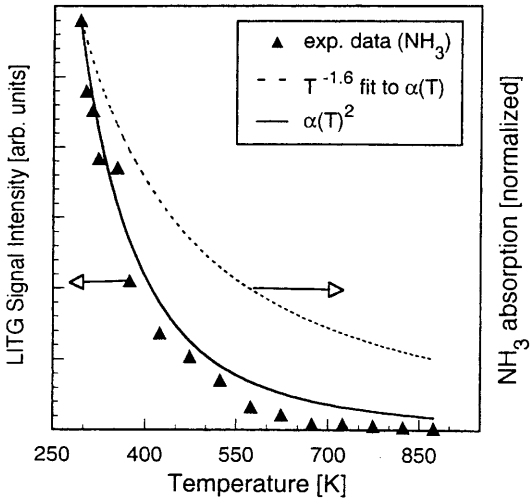

Fig. 9. Temperature dependence of NH_3 LITG signal intensity at 0.1 MPa total pressure: Experimental data from Fig. 4 (*filled triangles*; *left ordinate*). A comparison is shown with the calculated integrated ammonia absorption coefficient $\alpha(T)$ (right ordinate) within the linewidth of the CO_2 laser (*dashed line*: fit with T^{-n} function, *solid line*: $\alpha(T)^2$). The *curves* for the absorption coefficients are normalized to the first experimental data point at room temperature

from Fig. 4. Therefore, most of this signal intensity decrease with increasing temperature can be ascribed to the reduced excitation efficiency of ammonia due to the decreasing populations of energy levels involved in the absorption of the exciting laser radiation. Considering the predictions of [7], together with the $T^{-3.2}$ dependence of α' leads to an overall temperature dependence of $T^{-7.2}$ which disagrees with the experimental observations.

Other factors that influence the temperature dependence of the LITG signal intensity have not been considered: the efficiency for creating the thermal grating is controlled by the VT rate constants which is temperature dependent. For C_2H_4 the VT relaxation rate constant changes as $T^{-1/3}$ [19], and the heat conduction coefficient κ for N_2 increases by a factor of 1.6 in the temperature range 300–500 K.

The pressure trends in the data are roughly consistent with the $\sigma^2 p^2$ scaling predicted by (7). The absorption cross section is inversely proportional to pressure when the monochromatic laser is tuned to line center of an isolated, homogeneously-broadened transition. However, the cross section has a weaker pressure dependence when contributions from nearby lines are significant, or when Doppler broadening is of the same order as homogeneous broadening. In fact, the cross section can actually increase with pressure if the laser is tuned away from resonance. Thus, without further details regarding the precise relative tuning between the laser and the nearby transitions and without access to a detailed database for computing C_2H_4 absorption spectra, the agreement between experiment and theory can be considered to be consistent, but not fully understood.

Qualitatively the computed temporal LITG traces (Fig. 2) compare well with the experimental data (Fig. 6). As pressure is increased and thermal diffusion is slower, both experiment and theory show a marked change in the shape of the LITG signal pulse. Quantitatively, the comparisons are not as satisfactory. For example, the 2.2-MPa trace in Fig. 6 has a computed thermal diffusion time of $\tau_{th} = 961\,\mu s$ (see Table 1). Yet, the experimental trace agrees most closely with the $\tau_{th} = 2000\,\mu s$ calculation. This dicrepancy may be caused, in part, by the slow time response (127 μs) of the LITG signal detector which has not been taken into account in the analysis. Errors in determining the exact temporal shape of the CO_2 laser pulse likely contribute to this discrepancy, as do uncertainties in the angle between the grating forming beams (recall that the thermal diffusion time varies as the inverse square of the angle between the pump beams).

5 Conclusions

There still is a lack of sensititve, nonintrusive and species-specific laser diagnostics techniques in flames for the spatially resolved detection of hydrocarbons and other polyatomic molecules which exhibit low fluorescence quantum yields and, therefore, make otherwise sensitive methods such as laser-induced fluorescence (LIF) less favorable. The mid-infrared laser-induced thermal-grating technique introduced in the present study might be a suitable solution, especially at high pressure. For this technique a CO_2 laser, as used in the present experiments, constitutes a simple and versatile excitation source with a multitude of spectral lines in close coincidence with characteristic absorption features of polyatomic molecules. To make unambiguous assignments for a certain detected species, spectral patterns at a multitude of CO_2 laser transitions need to be recorded [21, 22]. Due to the directional properties of the signal beam with its accompanying remote detection capability, samples can be probed without interference from thermal background radiation of the flame environments. For quantitative measurements, however, the detailed pressure and temperature dependence of the LITGS signal intensity for each species needs to be known, either from a theoretical model or via calibration experiments. So far, only qualitative agreement with theory in the pressure and temperature dependencies as well as the temporal evolution of the LITG signal have been achieved. For C_2H_4 and NH_3 the present results indicate a strong temperature dependence of the thermal LITG signal intensity between 300 and 700 K. This property, in combination with a fast wavelength-switching technique of the excitation frequencies might be used with advantage, for example, two-line thermometry applications in the preheating zone of combustion events.

For a better understanding of the LITG signal behavior with pressure and temperature a tunable and short-pulse CO_2 laser would be of great value. Finally, in high-pressure environments, long laser-pulse durations appear to be more efficient than shorter ones for species detection with LITG spectroscopy.

Acknowledgements. This work was supported by the EU BRITE EURAM III project and the Deutsche Forschungsgemeinschaft (DFG). Valuable discussions and guidance in the experimental part of this work by H. Latzel is gratefully acknowledged.

References

1. H.J. Eichler, P. Günter, D.W. Pohl: *Laser-induced Dynamic Gratings* (Springer Series in Optical Sciences, Springer, Berlin, Heidelberg 1986)
2. K.A. Nelson, D.R. Lutz, M.D. Fayer, L. Madison: Phys. Rev. B **24**, 3261 (1981)
3. M.S. Brown, P.A. DeBarber, J.S. Maggart, R.W. Pitz, R.L. Farrow, P.H. Paul: 33rd Aerospace Science Meeting & Exhibit, Reno, Jan. 95, AIAA paper No. 95-0425

4. E.B. Cummings: Opt. Lett. **19**, 1361 (1994)
5. A.P. Smith, G. Hall, B.J. Whitaker, A.G. Astill, D.W. Neyer, P.A. Delve: Appl. Phys. B **60**, 11 (1995)
6. P.M. Danehy, P.H. Paul, R.L. Farrow: J. Opt. Soc. Am. B **12**, 1564 (1995)
7. S. Williams, L.A. Rahn, P.H. Paul, J.W. Forsman, R.N. Zare: Opt. Lett. **19**, 1681 (1994)
8. H. Latzel, A. Dreizler, T. Dreier, J. Heinze, M. Dillmann, W. Stricker, G.M. Lloyd, P. Ewart: Appl. Phys. B **67**, 667 (1998)
9. A. Dreizler, H. Latzel, T. Dreier, A. Koch, J. Wolfrum: Ber. Bunsenges. Phys. Chem. **100**, 1678 (1996)
10. C.H. Lambeau, A. Fayt, J.L. Duncan, T. Nakagawa: J. Mol. Spectr. **81**, 227 (1980)
11. NH_3 absorption spectra in the vicinity of the exciting CO_2 laser lines were calculated at 1 atm with the HITRAN 96 data base and software (ONTAR Corp., North Andover, MA)
12. P.H. Paul, R.L. Farrow, P.M. Danehy: J. Opt. Soc. Am. B **12**, 384 (1995)
13. R.C.L. Yuan, J.M. Preses, G.W. Flynn: J. Chem. Phys. **59**, 6128 (1973)
14. A. Arnold, B. Lange, T. Bouché, T. Heitzmann, G. Schiff, W. Ketterle, P. Monkhouse, J. Wolfrum: Ber. Bunsenges. Phys. Chem. **96**, 1388 (1992)
15. A. Olafsson, M. Hammerich, J. Henningsen: Appl. Opt. **31**, 2657 (1992)
16. J. Förster, T. Hagen, M.V. Hoesslin, J. Uhlenbusch: Appl. Phys. B **62**, 263 (1996)
17. J. Warnatz, U. Maas, R.W. Dibble: *Combustion* (Springer, Heidelberg 1996)
18. L. Giroux, M.H. Back, R.A. Back: Appl. Phys. B **49**, 307 (1989)
19. R.C.L. Yuan, J.M. Preses, G.W. Flynn: J. Chem. Phys. **59**, 6128 (1973)
20. F.E. Hovis, C.B. Moore: J. Chem. Phys. **69**, 4947 (1978)
21. R.R. Patty, G.M. Russwurm, W.A. McClenny, D.R. Morgan: Appl. Opt. **13**, 2850 (1974)
22. S.T. Persijn, R.H. Veltman, J. Oomens, F.J.M. Harren, D.H. Parker: Appl. Spectrosc. **54**, 62 (2000)